A comparison of dispersion models for the LNG dispersion at port of Koper, Slovenia

A comparison of dispersion models for the LNG dispersion at port of Koper, Slovenia

Gerbec Marko[a, *], Vidmar Peter[b], Pio Gianmaria [c], Salzano Ernesto [c]

[a] Jozef Stefan Institute, Jamova 39, 1000 Ljubljana, Slovenia

[b] Faculty of Maritime Studies and Transport, University of Ljubljana, Pot pomorščakov 4, 6320 Portorož, Slovenia

[c] Dipartimento di Ingegneria Civile, Chimica, Ambientale e dei Materiali, Università degli studi di Bologna, Via Terracini 28, 40131 Bologna, Italy

* Corresponding author. Tel.: +386 1 4773169. E-mail address: marko.gerbec@ijs.si

Abstract

The challenges of ensuring green shipping and green ports force ports to adequately and safely implement engineered systems for the distribution and supply of LNG in port areas that meet the requirements of Seveso Directive. As the process of LNG bunkering is only seemingly similar to classical oil bunkering or liquid cargo, the handling of the technical and safety challenges is much more subject to investigation. In this work, the dispersion part of the consequences of LNG release, pooling, evaporation and dispersion during the future bunkering operation in the port of Koper, Slovenia, where the populated area (city) is located in close proximity. We follow the comparison of three different tools, namely the model Unified Dispersion Model (UDM) implemented by the software PHAST from DNV-GL® and two CFD (FDS - Fire Dynamics Simulator from NIST and Ansys Fluent®) in the same case scenario. Geometry, initial and boundary conditions are assumed to be the same as far as possible according to the limitations of the respective software tools. The simulation tools are first applied to a flat terrain model and later the models of CFD are compared, including the 3D geometry of the dock site in real size, with two relevant wind directions. The effects of evaporation rates on water and turbulence on CFD estimates are also given and numerically tested. The results of the applied models provide valuable information for further establishment of similar LNG leakage and dispersion models for simulation in ports or similar facilities.

Keywords: LNG, bunkering; risk assessment; dispersion; CFD; UDM model

Abbreviations

CFD	Computational Fluid Dynamics
FDS	Fire Dynamics Simulator
LNG	Liquefied Natural Gas
UFL	Upper Flammability Limit
LFL	Lower Flammability Limit
PTS	Pipeline To Ship bunkering system (also Shore to Ship)
STS	Ship To Ship bunkering system
TTS	Truck To Ship bunkering system
UDM	Unified Dispersion Model

1 Introduction

Pollution prevention in the maritime industry (IMO, 1997) has led to significant interest in the use of Liquefied Natural Gas (LNG) as an alternative clean maritime fuel instead of fuel oil. However, conversion to LNG fuel is a lengthy process that faces many obstacles, such as major technical differences in engines, logistics, and supply infrastructure. LNG is a cryogenic liquid produced by cooling natural gas to about -163 °C (110 K) to reduce its volume by a factor of about 600. While the safety of large LNG carriers and their associated regasification terminals has been the subject of much study in the past, the coming widespread use of LNG as a fuel will require the design of marine bunkering operations, usually in or around port areas. This brings a new dimension to the safety of ship operations in ports and has been the subject of extensive literature reviews (Aneziris, 2020). Several standards, guidelines and regulations related to LNG fuel technology are rapidly becoming available to cover the technical and organizational requirements. In addition, the limited amount of scientific work on risk assessment indicates that there are still many unanswered questions due to the specific properties of LNG, e.g.: Vapours have an initial negative buoyancy, the evaporation rate during spills is still uncertain, or the vapour can sustain rapid phase transition phenomena (RPT). In addition, the effects of light hydrocarbons in LNG composition affect flammability limits and other properties (Sandia, 2014; Cleaver et al., 2007; Pio and Salzano, 2018)).

The prime issue in planning LNG bunkering operations in ports is the concept of safety distances (exclusion zones) that need to be established and ensured to prevent potential damage to the adjacent port or other civil activities in the vicinity (ISO, 2015). Recent work and studies (Alterman, 2005; Aneziris et al., 2014; Sun et al., 2017; Jeong et al., 2017, 2018; Animah and Shafiee, 2020; DNV, 2012; Rambøll, 2013) suggest that this is a challenging task - here are the key points:

- During the bunkering process (either truck-to-ship (TTS), pipeline-to-ship (PTS), or ship-to-ship (STS) design), a potential LNG release at the bunker interface (loading hoses or arms used) is most likely due to a connection failure (internal or external cause). Various leak sizes or ruptures may occur, of which a full bore rupture at the liquid phase line should be considered as a conservative option.
- Released LNG forms a jet and flows into the pool that forms (onshore or offshore) below the release point. Due to the much higher temperature of the environment, the LNG will quickly vaporize and form a flammable cloud that will be carried away by the wind

(note that RPT - a rapid phase transition, a local physical explosion at sea is also possible).

- The flammable cloud is subject to movement and dispersion in the ambient air, depending on terrain geometry (e.g. port infrastructure, ships, coastal elevation, etc.).
- When the flammable cloud is ignited, it burns as a flash fire back to the source, resulting in one or more additional phenomena such as jet fire, pool fire.

According to these key points, the flash fire is the most credible scenario in the case of delayed ignition of vapour cloud of LNG. That is, the flame propagation is rarely considered to be able to accelerate and, consequently, to generate severe pressure wave in open environment, as in for the vapour cloud explosion (VCE) scenario. This assumption is soundly based on the low overall reactivity of cryogenic methane cloud, hence at low temperature and often forming non-homogeneous stratified layers (Pio and Salzano, 2018). Furthermore, bunkering areas are rarely characterized by highly congested geometry, which is an essential condition for the flame acceleration (according to the Schelkin effects, see CCPS (1994) and Tufano et al. (1998) for more details).

The purpose of this paper is to address three of the above issues. First, a review of the available studies that report on the methods and tools used to evaluate the evaporation rate from a pool formed over water (sea). Indeed, the work and experimental data suggest that the formation of the LNG pool over deep water is a complex process and that its modelling and the consideration of the total evaporation flux (starting point for the dispersion of the flammable gas) deserves special attention (Fay, 2007; Horvat, 2018). Two, port-specific safety studies (e.g., DNV, 2012; Rambøll, 2013) commonly use integral dispersion models such as the Unified Dispersion Model (UDM) implemented in the PHAST software (DNV GL, 2017a, 2020). These models cannot account for complex terrain geometries and spatial obstacles in the model domain, as mentioned in the points above. To this end, many papers and some case studies also use some of the available CFD modelling tools that can adequately account for complex geometry in a 3D model of the case (Hansen et al. 2009; Jeong et al., 2017, 2018; Horvat, 2018; Park et al., 2018; Rambøll, 2013; Scandpower, 2012).

Finally, as suggested by Park et al. (2018) and Horvat (2018), the dispersion is largely influenced by the geometry of both the ships and the port facilities, as well as the actual wind speed and direction. This means that dispersion modelling must always be case-specific, down to each potential micro-location, leading to difficulties in establishing generic safety distances for the specific engineering arrangements involved in bunkering.

In this regard, the paper will explore these issues in the context of realistic ship-to-ship (STS) bunkering operations between a bunkering vessel and a large container ship. In particular, we will examine the available information on the LNG evaporation rate from the pools formed above the sea surface, the available UDM dispersion model through the PHAST tool (DNV GL, 2017a, 2020) and two CFD dispersion modelling tools, namely the Fire Dynamics Simulator (FDS) from National Institute of Standard and Technology (NIST) of the USA (McGrattan et al., 2018) and the Ansys Fluent® (Ansys Fluent, 2021), as well as the effect of bunkering micro-locations and local meteorological conditions on the dispersion into the ambient air. To our knowledge, such comparative modelling of potential LNG evaporation and dispersion has not yet been reported in the context of assessing safe distances for bunkering operations.

In Section 2.1, we will review the available literature on experimental and modelling information on realistic LNG evaporation rates for spills that form a pool over deep water and propose new data for consideration. In Section 2.2, we will explain the UDM dispersion model used (part of the PHAST tool) through the details of the case study (Section 3). In Sections 2.3 and 2.4, we will explain the approach to modelling the dispersion using two alternative CFD models, namely FDS and Fluent. In Section 3, we will present the modelling case situation of LNG STS bunkering that will take place in the future in the port of Koper, Slovenia. We will cover selected alternative micro-locations, taking into consideration all relevant site characteristics (terrain, sensitive areas and meteorological data) and the details of the LNG release scenario. In Section 4 we will present and discuss the results, starting with the UDM modelling, followed by a comparison of the results of UDM, FDS and Fluent models for the case of flat terrain and finally the results of FDS and Fluent for the realistic case of terrain, micro-locations and meteorological conditions of the port of Koper. In Section 5, conclusions are given on the case modelling results, the epistemic uncertainties addressed and the applicability of the results to the development of safety distances.

2 Methods, tools and data used

2.1 Evaporation rate from pools over deep water

Few data for small scale LNG releases – which may be considered typical for STS operations - are available in the literature. According to Luketa-Hanlin et al. (2006), the mass evaporation rate m''_{ev} can vary between 0.029 to 0.185 kg s^{-1} m^{-2} as a mean value. This range of values could be considered for CFD or other purposes, in the absence of more accurate values. Quite clearly, uncertainties arise from pool dimension (effect of Reynolds number), pool formation (discharge

rate) and atmospheric conditions. The given range is however confirmed by several experimental tests. On average, the pool is considered at 112 K, the atmospheric and water (when applicable) temperatures are 298 K and 293 K, respectively. The experimental tests of the Bureau of Mines, as reported by Burgess et al. (1972) have evaluated a value of 0.181 kg s^{-1} m^{-2} and 0.155 kg s^{-1} m^{-2}. Sandia (2004) measured a value of 0.195 kg s^{-1} m^{-2}. On the contrary, Luketa-Hanlin (2006), in the well-known test of Maplin Sands measured 0.085 kg s^{-1} m^{-2} (possibly due to the large pool scale and the inverse relation with the pool radius). Most of the simplified studies have adopted 0.181 kg s^{-1} m^{-2} as a reference value, following a conservative approach. However, similar evaporation rates have been largely associated with the case of LNG pool fire as well (Fay, 2006). Hence, the implementation of similar values for dispersion/potential flash fire scenario implies an arguable assumption of the negligible effect of heat generated by the flame above the pool on the evaporation. In this view, the adoption of a more fundamental-based approach is desirable. Among the others, Klimenko's model (Klimenko, 1981) estimates the heat transfer coefficient based on Nusselt, Prandtl, and Archimedes numbers in case of liquid evaporation on a calm liquid surface. The presence of the latter dimensionless number suggests the significance of the effect of a dense cloud of fuel vapours in the proximity of the pool on the evaporation rate. Conrado and Vesovic (2000) have validated the abovementioned model for the LNG case, as well, obtaining an evaporation rate of 0.072 kg s^{-1} m^{-2}. Eventually, the effect of water turbulence can be assessed separately. Indeed, an experimental campaign on lab-scale facilities conducted by Morse and Kytömaa (2011) have observed an almost linear trend for the water surface turbulence intensity for LNG evaporation rate. Experimental contingencies (i.e., ice formation) have limited the analysis to velocity fluctuation smaller than 0.1 m s^{-1}, in agreement with theoretical treatment reported by Vesovic (2007) supposing an abrupt decrease in the surface temperature of water and ice formation in the case of confined and shallow-water surfaces. Nevertheless, in the first approximation, an extrapolated value has been reported for the case of null velocity fluctuation, assuming a linear trend (i.e., 0.053 kg s^{-1} m^{-2}). The reported value results in substantial agreement with the theoretical-based estimation reported by Conrado and Vesovic. Eventually, we will consider two values: the conventional at 0.181 kg s^{-1} m^{2}, and the alternative at 0.053 kg s^{-1} m^{-2}.

2.2 UDM dispersion model & tool used

Standard off the shelf methods and tools are widely used to model the consequences of the releases of hazardous materials. In that respect, we used an integrated software package DNV GL PHAST version 8.22 (DNV GL, 2020). The programme tool already contains a database

with the properties of pure substances. The programme uses the Unified Dispersion Model (UDM) to model jets, dense, buoyant and passive dispersion including droplet rainout and re-evaporation (DNV GL, 2017a). The model allows for continuous, instantaneous, constant finite-duration, and general time-varying releases; nevertheless, time-varying releases are treated as a series of a maximum of 10 pseudo-steady-state steps, thus providing only a rough representation of the trend over time of the release characteristics.

The modelling was limited to the use of the user-defined release case, prescribing the LNG release rate & duration at the set process and case conditions (later reported in Table 1), resulting in data on the LNG pool formation and downwind distances to UFL, LFL and LFL/2 concentrations in ambient air (16.5 %, 5 % and 2.5 % vol., respectively).

Related to the topic of this paper it is worth to note that the built-in modelling considers the conventional LNG evaporation rate from a pool on the water at 0.18 kg s^{-1} m^{-2} (DNV GL, 2017b), adopted from Burgess et al. (1972).

2.3 CFD dispersion modelling using FDS tool

A simplified 3D layout, representative of the bunkering terminal and nearby city, was implemented in FDS for the characterization of accidental release of LNG on water, by using the user-friendly interface PyroSim (McGrattan et al., 2020). The time-depending properties were visualized using the SmokeView tool (SMV). FDS is an open-source software developed by the National Institute of Standards and Technology (NIST) suitable for the modelling of low Mach problems. It is based on the Large Eddy Simulation (LES) approach as a low-pass filter for Navier-Stokes equations and it has been extensively validated for accidental release of LNG (Sagaut et al., 2002; Zhang et al. 2016, Pio et al. 2019, Zheng et al. 2019).

2.3.1 General description of the geometry

Figure 1 shows the 3D computer-aided design (CAD) model for the geometry model general arrangement including the LNG bunkering ship, the port basin, and the nearby town. The geometry is imported into the PyroSim software (McGrattan et al., 2020) where the natural gas dispersion is simulated with FDS code. The geometry is designed in a real size dimension and covers the area of the container terminal, the basin, the cruise ship terminal and the populated area of the town centre. The main obstructions that could influence the dispersion of the gas are included in the 3D model and represent container blocks, warehouses, and other elevated buildings. All the obstructions are geometrically square blocks and are thermally inert. The Triple E class container ship is placed by the pier 1 berth 7 and is moored on its starboard side

with a 100 m long LNG bunkering ship. The lateral distance between ships is 4 meters what forms a partially closed water channel with an area of about 300 m^2. The geometry of the town centre is designed according to the actual altitudes and the position of buildings and main streets. The configuration of the town terrain is a hill shape and has the highest point about 15 meters on the side towards the container terminal. The altitude is then dropping to 3 m at the boundary of the designed town geometry.

2.3.2 Scenario modelling

The gas dispersion caused by LNG leaks during bunkering accident was simulated with the Fire Dynamics Simulator (FDS) (McGrattan et al., 2018). The gas dispersion is simulated using LES in FDS where Favre filtering is used in the momentum equation, mass, energy, and species combined with state equations for ideal gases. In the present study, the source term $\dot{m}_{\alpha}''$, the mass flux of the methane species is added to the species transport equations and is defined on the boundary of the modelled LNG pool. The simulation of combustion is avoided in this study as the main interest is to find the area that could be affected by the concentration of the methane gas.

The 3D domain size is 1115×953×83 m and was discretized with finite volume meshes having a resolution of 2×2×0.7 m. The space discretization of the mass equations, motive quantity and heat energy is derived with the method of finite difference in the central differential scheme in a square net. The time discretization of the transfer equations is made on an explicit scheme of predictor-corrector. After the grid independence analysis for gas dispersion, a total of 24,000,000 cells was used, and the cell aspect ratio was set to 3×3×1 in the Cartesian coordinate system. In x and y directions the size of the cell is not optimal but fits the simulation convergence criteria.

The transient calculation is set to 400 seconds, as the results showed later the LFL/2 concentration is not any more present after that time (in fourth micro-simulation reported in coming section 4.3.1 this was doubled). The main points of the observations are the methane concentration distributions at 5 and 2.5 % by volume, corresponding to the LFL and LFL/2 concentrations, respectively.

2.4 CFD dispersion modelling using Fluent tool

Other than the turbulence sub-model, the numerical characterization of cloud dispersion performed by using Fluent utilized the same boundary conditions and domain defined

previously for the FDS case. Indeed, accidental releases of LNG either in the presence or absence of obstacles representative for the port layout were tested under different atmospheric conditions and by using different source sub-models. In this case, the Reynolds Average Navier-Stokes (RANS) approach has been implemented using the k-ε closure model. Smaller accuracy in spatial and temporal discretization should be required with respect to the LES approach, due to the number of eddies evaluated. However, the differences in the filtering process have the potential to generate significant variations in the proximity of walls. Readers may refer to the technical guide of the mentioned software for a detailed discussion on the adopted governing equations and posed hypotheses.

3 Case study

The port of Koper is a multi-purpose port located in the north Adriatic sea. Located directly in contact with the old town centre, it is always subjected to safety assessments, as the port activities have potential risks to the neighbouring population. The strategy of the port is also to provide, in the near future, the possibility of LNG bunkering for all or at least some types of ships. Potentially, the most promising are container ships and cruise ships. Terminals for both types of ships are located in basin 1, on the north side (berth 7) serving the container ships and the passenger terminal on the south (berth 1) serving cruise ships. The closest populated area is about 50 meters south of berth 1. The houses in the old town are about 10 m above sea level. The case study assumes the two most probable positions of receiving and bunkering ships, namely, berth 1 and berth 7. The receiving ships are assumed to be large: the container ship is a size of a triple E (length of 400 m) and a passenger cruise ship length is about 350 m. The height of the receiving ships is also important, because compared to the size of a bunkering ship, they represent a wind barrier that can keep them in a leeward from the wind. The situation and 3D model are presented in Figure 1.

(Figure 1)

3.1 Meteorological situation

The relevant meteorological data for the Port of Koper were obtained the from port's automatic meteorological stations. The wind rose profile for the year 2020 is presented on Figure 2. It can be concluded that the dominant wind speed is at about 2 m/s, the prevalent wind direction is

from the east-south-east (direction at about 110°), followed by west-north-west direction (direction at about 300°).

Accordingly, the wind speed was set to 2 m/s at the height of 10 m above the sea and the atmospheric boundary layer is assumed using Monin-Obukhov similarity theory (McGrattan et al., 2018). Both mentioned wind directions were further considered in the modelling.

The initial temperature of the atmosphere was set to 20 °C at 50 % relative humidity. The boundary land surface was created under adiabatic conditions, and the other boundary conditions were set as open to simulate general inflow and outflow conditions. The sea surface is applying the water thermal properties to simulate the heat transfer between cold natural gas and sea surface.

(Figure 2)

3.2 Release scenario

The technologies usually consider operations with LNG stored at about -164 °C (109 K) and 6 bar pressure difference at the ship-to-ship bunkering interface (Rambøll, 2013; Scandpower, 2012). The hoses used are DN150 size and a typical flow rate considered is 350 $m^3 h^{-1}$ delivered by the submerged centrifugal pumps. In the case of the hose rupture, the release from the liquid phase branch is the most important and due to the pumps impeller, the flow rate can increase due to the pressure drop maximum by a factor of 1.2 to 1.5 (Rambøll, 2013). In this paper, we consider a factor of 1.3. Considering the LNG density of 420 kg m^{-3} this brings to the expected release rate of about 53.2 kg s^{-1}. On the other side, there are many safety systems planned to stop small and large leaks, including the presence of the operators. As a rather conservative estimation, we consider that the rupture is stopped within 120 s from the start.

The most important input parameters used in modelling by all three tools are summarized in Table 1.

(Table 1)

Following the spill of LNG over the sea surface, transient evaporation and boiling of the natural gas starts. However, the remaining LNG spreads over the sea surface as a pool. The modelling of the pool formation and natural gas evaporation into the dispersion modelling is integrally done within the DNV GL PHAST tool. Results obtained in the coming section 4.1 suggest that the pool reaches the maximum size at 120 s and the largest area of about 300 m^2 considering conventional pool evaporation rate of 0.18 kg $s^{-1} m^{-2}$. In FDS and Fluent models, we considered

the LNG pool formation data as presented in Figure 3 due to the necessary modelling simplifications in the pool area evaporation.

(Figure 3)

The LNG pool forms in a channel between both ships (see description of the geometry in section 2.3.1) that is closed with a floating barrage at both exits as well as around both ships.

4 Results and discussion

4.1 UDM dispersion model

LNG pool formation, evaporation and dispersion results obtained using an integrated UDM modelling tool are summarized in Table 2 and graphically presented as iso-concentration contours over a map of the case area for two micro-locations and two wind directions in Figure 4. Results suggest that the LNG pool should reach the maximum diameter of about 28 m in about 40 s (in a case of late ignition) and that it should evaporate completely within 15 s after the release has terminated. Considering the dispersion in the ambient air, for example, the LFL and LFL/2 concentrations are to be reached downwind at about 205 and 377 meters, respectively. Figure 4 suggest that the flammable could reach large areas within the port, e.g., container terminal just north of berth 7, or fruit terminal just west to berth 1, as well as areas outside the port (presented as dashed red line). In comparison, the west-north-west wind (at 300°) (Figure 4 situations B and D) is a worse alternative to the east-south-east wind (at 110°) (Figure 4 situations A and C) for both alternative berth locations. Needless to say, the UDM modelling does not consider the terrain elevation in the case area, e.g., port shore, port buildings and city of Koper's elevation, streets and squares.

(Table 2; Figure 4)

4.2 Comparison of the results considering the flat terrain

The validation geometry that consists of a methane-emitting source and a flat terrain was used by two CFD model results (FDS and Fluent) and compared to the UDM model results (DNV GL PHAST). The source represents the confined LNG source of 300 m^2 with a conventional evaporation rate (0.18 kg s^{-1} m^{-2}). The domain and the spatial discretization is of the same size and the same number of grid cells, described above. The observation of results is focused on

the calculation of the gas dispersion parameters: the cloud distance vs time at LFL and LFL/2 concentrations is presented in Figure 5, the cloud area vs time at LFL and LFL/2 concentrations is presented in Figure 6, and the cloud height vs distance at 160 s is presented on Figure 7.

Figure 5 show the calculated cloud front side distances related to LFL and LFL/2 concentrations are to some extent similar during the dispersion time for all three models. Maximum distances to LFL concentration related to UDM, FDS and Fluent models are about 210, 220 and 150 m, respectively. The distance-time profiles vary more clearly even if the order of magnitude is consistent with the given uncertainties: the cloud dissipates at about 200, 270 and 303 s, according to the UDM, FDS and Fluent models, respectively. Maximum distances to LFL/2 concentration related to UDM, FDS and Fluent models are about 380, 570 and 310 m, respectively. The cloud dissipates at about 273, 470 and 330 s, according to the UDM, FDS and Fluent models, respectively.

Figure 6 suggest that the maximum cloud area is comparable between UDM and FDS models (about 15,000 and 35,000 m^2 considering LFL and LFL/2 concentrations, respectively; however, for UDM we have only values at the max. cloud size time), while for Fluent maximum cloud area is about 950 and 1800 m^2, respectively.

Figure 7 provides part of the explanation for the differences among the models. Considering the LFL concentration at 160 s, all three models report maximum cloud height at about 6 m. It is worth noting that the height profile of UDM diverges from the profiles of FDS and Fluent. Interestingly, considering LFL concentration, UDM and FDS models report the same distance to height 0 m (200 m), whereas Fluent reports a value of 250 m. If considering LFL/2 concentration, the values are closer: FDS and Fluent models report 250 m, whereas UDM shows a value of 270 m. To conclude, while the cloud profiles differ, the differences among the cloud front distances reached are relatively minor.

(Figure 5, Figure 6, Figure 7)

4.3 Results considering the Port of Koper real terrain

The configuration of the berths and moored ships are pre-determined by port. Geometrically, most of the influence on the fluid dynamics around the ship comes from the ship type and its particular freeboard. The large freeboard represents a barrier to a downwind flow and a significant source of vortices on a leeward side. This is mostly the case of a container ship exposed to north or north-west wind. A series of three micro-simulation results are presented considering the conventional LNG evaporation rate of 0.181 kg s^{-1} m^2. The first is when the

container ship is moored at berth 7 at the north side of basin 1 and the wind direction is from 300°. The second and the third micro-simulations locate the cruise ship at the south side of basin 1 at berth 1 and the wind directions are from 300° and 110°, respectively. Video recordings of micro-simulations are available in section Supplementary material.

The first micro-simulation is presented as a set of methane concentration snapshots in time obtained by the FDS model in Figure 8. The figures present the top view of the cloud, however the longitudinal cross section is presented separately to indicate the influence of the ship hull to the cloud movement. The presence of the ship importantly influences the dispersion of the gas cloud, its shape and length. The figure shows the LFL cloud concentration at different time steps, but the shape of the cloud is even not directed downwind but dilutes due to the vorticity before reaching the mainstream of the wind.

The comparison of downwind distance and cloud area to LFL concentration vs time for FDS and Fluent models for this micro-simulation is presented in Figure 9. We can observe that both models agree very well related to the downwind distance vs. time profiles, however, Fluent reports much lower cloud area figures. We can also observe that the maximum cloud distance is about up to 30 % lower in comparison to the case of considering flat terrain (previous section).

(Figure 8, Figure 9)

The second micro-simulation is presented as a set of methane concentration snapshots in time obtained by the FDS model in Figure 10. The dispersion of gas cloud concentration is observed for the LFL concentration. The cloud is directed downwind along the shipside and reaches a distance of about 400 m from the pool. In this case, the cloud does not reach the shore area but remains and dilutes on a seaside. The comparison of downwind distance and cloud area to LFL concentration vs time for FDS and Fluent models for this micro-simulation is presented in Figure 11. The velocity of the cloud spread is near-constant along its path (FDS model). The area that the gas cloud covers is at most about 16000 m^2, which is more than three times larger than in the first micro-simulation, but close to the area from the case considering flat terrain (previous section). The reason is the dispersion of the gas is less influenced by environmental geometry. The ship's position alongside the direction of the wind acts as a duct or channel and is not a source of larger vortices that would contribute to faster dispersion of the gas. This influence is observed especially because the size of the ship is much larger than the bunkering ship and the pool size, and geometrically covers most of the observed gas cloud. On the other hand, estimations obtained by Fluent indicate a flammable region limited to the ship boundaries

(i.e., to the duct formed by the obstacles). The comparison of the area and size in the downwind direction suggests that a less effective dispersion can be assumed with respect to the other models employed in this work since only the direction driven by wind is characterized by similar results. Considering that the reported results refer to a given distance from the sea level, this discrepancy can be attributed either to the different estimation of fuel density with cryogenic temperature leading to higher cloud or larger average concentration of the fuel within the cloud.

(Figure 10, Figure 11)

The third micro-simulation is presented as a set of methane concentration snapshots in time obtained by the FDS model in Figure 12. The dispersion of gas cloud concentration is observed for the LFL concentration. It can be observed that even if the wind is oriented towards the city the size of the container ship acts as a barrier and redirects the airflow along the seaside of the hull to the direction of the general cargo terminal (east). In any case, the gas cloud stays during the simulation within the port area limits.

The comparison of downwind distance and cloud area to LFL concentration vs time for FDS and Fluent models for this micro-simulation is presented in Figure 13. Data resulting from the LES simulations (i.e., FDS) indicate almost double downwind distances than the RANS case (i.e., Fluent), confirming the relevance of turbulence modelling for the evaluation of dispersion scenarios. Indeed, less accurate sub-grids filtering the eddies as per the evaluation of the turbulence result in less effective mixing, leading to a higher concentration of fuel within the cloud, thus smaller flammable areas. The analysis of the cloud distances and area vs. time shows that the gas cloud reaches a distance of about 370 m and then disappears. The distance is similar to the second micro-simulation, even though the maximum area of the cloud is about 25 % smaller. The gas cloud is again canalised by the ship hull and is less perturbed, keeping the slender shape along the hull. The influence of the vorticity caused by faster gas dispersion is not visible and can be observed from the distribution of the cloud area during the simulation. The velocity of the cloud spread (distance, area) is near-constant along its path till the stop of the release at 120 s (FDS model). This indicates the cloud is not perturbed significantly during its dispersion.

Similar trends describing the evolution of the cloud along with the time were reported for the investigated scenarios, suggesting a limited impact due to the layout configuration.

(Figure 12, Figure 13)

The comparison of the presented results from different scenarios indicates that either the extension of the flammable area or the maximum downwind distance having a flammable mixture are mainly affected by the congestion, with a limited impact on the considered evaporation rate. Regardless of the implemented sub-model and layout, the evolution of the cloud size to time can be represented by three stages: initial growth, pseudo-steady state, and decay. However, after an initial phase, the presence of obstacles decelerates the growth phase and reduces the duration of the pseudo-steady state stage. Considering that the evaporation rate is kept constant at this stage, these trends imply that a higher average concentration of methane is reached within the cloud. Hence, the occurrence of stratified mixtures can be hypothesized. Hence, the estimation of the standoff distances in case of accidental release of cryogenic liquids is strongly influenced by the selected height from the sea level. Besides, regular cloud edges may be inferred by the smoothness of the reported trends from results deriving from Ansys Fluent, only. Hence, this observation is affected by the sub-model considered for turbulence.

4.3.1. Results on alternative evaporation rate

The fourth micro-simulation considers the geometry of the first micro-simulation (described in the previous section) and applies the alternative LNG pool evaporation rate of 0.053 kg s^{-1} m^{-2}. Assuming the same release conditions and same size of the pool, the overall pool evaporation rate lowers leading to its long lifetime. The considered pool overall evaporation rate and the cumulative amount vaporised vs time is presented in Figure 14.

(Figure 14)

The fourth micro-simulation is presented as a set of methane concentration snapshots in time obtained by the FDS model in Figure 15. The dispersion of gas cloud concentration is observed for the LFL concentration. We can observe that consideration of the alternative LNG evaporation rate extends the duration of the flammable cloud in the modelling domain considerably from about 300 s to about 750 s (compare to Figure 8).

Figure 16 presents the calculated distances to LFL concentration and cloud area vs simulation time for FDS and Fluent models. The maximum downwind distances are about 90 and 110 m, maximum cloud areas are about 3500 m^2 and 500 m^2, for FDS and Fluent, respectively. While

the difference in downwind distances is small (20 %), the profiles diverge, not mentioning the profiles of cloud area vs time.

(Figure 15, Figure 16)

Estimations from the first micro-simulation (with conventional LNG evaporation rate) - Figure 8 and Figure 9, with results from fourth micro-simulation (with alternative evaporation rate) - Figure 15 and Figure 16 can be compared for further insights. Results indicate that the maximum downwind distance of the cloud to LFL concentration is in the fourth micro-simulation case about 60 % longer and the maximum cloud area about 30 % larger than in the first micro-simulation. Besides, we can compare both related micro-simulations for FDS and Fluent in Figure 17 and Figure 18, respectively. We can observe that consideration of the alternative LNG evaporation rate extends the duration of the flammable cloud in the modelling domain from about 275 s to about 750 s (FDS) at +170 %, or from about 300 s to 750 s (Fluent) at +150 %. While the alternative evaporation rate is at –70 % of the conventional, the maximum downwind distance to LFL changes from about 160 m to 90 m (FDS) - thus by -44 %, or from about 150 m to 110 m (Fluent) – this by -27 %. The maximum cloud area at LFL concentration changes from about 5000 m^2 to 3500 m^2 (FDS) – thus by -30 %, or from about 700 m^2 to 500 m^2 (Fluent) – thus by about -30 %.

Hence, it is possible to conclude that the differences in maximum cloud distances and cloud areas are smaller than the reduction in the evaporation rate considered. The reason for that is that the same amount of gas evaporates into the air, however at about 70 % lower overall rate from the formed pool. That is next related to the relatively stable wind conditions that allow the formation of a homogeneous cloud. Its dispersion is mostly influenced by the vorticity downwind of the ship which allows larger air entrainment into the cloud. The leeward area of the ship acts as a shelter to the evaporated cloud that is kept low above the sea surface due to a low temperature. The movement of the cloud in the first period after formation is governed mainly by the negative buoyancy, which is thermally dependent. This is why the dispersion is limited, keeping the gas cloud compact and allow its spread to a relatively large size comparing to reduced evaporation rate. The gas cloud accumulated along the sheltered area of the ship evenly enters the vorticity zone downwind the ship and allows larger air entrainment over the boundary of the gas cloud and consequently faster dilution.

5 Conclusions

The simulations of LNG spill and gas dispersion presented in this paper are limited to the most credible scenario. The limits of the spill are based on guidelines and standards for marine equipment engineering and are assumed to apply to technical failures and marine accidents in ports. In these cases, LNG spill is predictable and controlled by the ship safety system including emergency shutdown of the bunkering process. The leakage time, spill quantity and pool area boundaries assumed in the model are derived from the assessed bunkering process and represent the boundaries for the safety assessment. According to these assumptions, the three case micro-simulations are verified using three different models, one UDM and two CFD. The results show that all three models give comparable results for the gas dispersion distance in flat terrain, although Fluent calculates a smaller area of the cloud in all three cases. The results of the analysis of the results show a significant influence of the geometry around the LNG pool, i.e. the large ship acts as a barrier increasing the vorticity when it is upwind of the pool and acts as a channel when it is downwind of the pool. The UDM model does not account for the heights of the geometry and is therefore not reliable for LNG spills where the vaporized gas cloud remains stratified a few meters above the ground and is also strongly influenced by lower structures such as piers, houses and moored ships. CFD should be considered for gas dispersion in these cases with a defined gas evaporation rate obtained from experimental tests or simulated separately and validated for a specific spill case.

Acknowledgement

The authors gratefully acknowledge financial support from Adriatic-Ionian Program INTERREG V-B Transnational 2014-2020, project #118: SUPER-LNG - “SUstainability PERformance of LNG-based maritime mobility”.

Supplementary material

Micro-simulation 1.wmv – video recording of the first micro-simulation using FDS in section 4.3

Micro-simulation 2.wmv – video recording of the second micro-simulation using FDS in section 4.3

Micro-simulation 3.wmv – video recording of the third micro-simulation using FDS in section 4.3

Micro-simulation 4.wmv – video recording of the fourth micro-simulation using FDS in section 4.3.1

(Link to files: Micro-simulation 1.wmv, Micro-simulation 2.wmv, Micro-simulation 3.wmv and Micro-simulation 4.wmv)

References

Alderman, J.A., 2005. Introduction to LNG Safety. *Process Safety Progress*, 24, 3. https://doi.org/10.1002/prs.10085

Aneziris, O., Koromila, I., Nivolianitou, Z., 2020. A systematic literature review on LNG safety at ports. *Safety Science*, 124, 104595. https://doi.org/10.1016/j.ssci.2019.104595

Aneziris, O., Papazoglou, I.A., Konstantinidou, M., Nivolianitou, Z., 2014. Integrated risk assessment for LNG terminals. *J. Loss Prev. Process Ind.* 28, 23–35. https://doi.org/10.1016/j.jlp.2013.07.014 .

Animah, I., Shafiee, M., 2020. Application of risk analysis in the liquefied natural gas (LNG) sector: An overview., *J. Loss Prev. Process Ind.* 63, 103980. https://doi.org/10.1016/j.jlp.2019.103980

Ansys Fluent, 2021. More info on Ansys Fluent Fluid Simulation Software at https://www.ansys.com/products/fluids/ansys-fluent crui

Burgess D., Biordi J., Murphy J., 1972. Hazards of spillage of LNG into water. *NAT. TECH. INFO. SERV.* https://apps.dtic.mil/sti/citations/AD0754498

CCPS, 1994. Guidelines for Evaluating the Characteristics of Vapor Cloud Explosions, Flash Fires, and BLEVEs, American Institute of Chemical Engineers (AIChE), Center for Chemical Process Safety, Wiley.

Cleaver, P., Johnson, M., Hob, B., 2007. A summary of some experimental data on LNG safety. *Journal of Hazardous Materials*, 140, 429–438. https://doi:10.1016/j.jhazmat.2006.10.047

Conrado C., Vesovic V., 2000. The influence of chemical composition on vaporisation of LNG and LPG on unconfined water surfaces. *Chem. Eng. Sci.*, 55, 4549–4562. https://doi.org/10.1016/S0009-2509(00)00110-X

DNV GL, 2017a. Report *THEORY Unified Dispersion Model* (for registered users).

DNV GL, 2017b. Report *THEORY Pool Vaporisation* (for registered users).

DNV GL, 2020. More info on PHAST and SAFETI software packages https://www.dnvgl.com/services/qra-and-risk-analysis-software-phast-and-safeti-1676 (27.8.2020)

DNV, 2012. *Report Port toolkit risk profile LNG bunkering*. Port of Rotterdam, Ministry of Infrastructure & Environment, Port of Antwerp, Port of Amsterdam and Zeeland Seaport. Report No./DNV Reg No.: PP035192-R2 Rev. 2, 28 August 2012.

http://www.lngbunkering.org/lng/sites/default/files/2012%2C%20DNV%2C%20Port%20Toolkit%20Risk%20Profile%20LNG%20bunkering.pdf

Fay, J.A., 2006. Model of large pool fires. *Journal of Hazardous Materials*, 136, 219-232. https://doi.org/10.1016/j.jhazmat.2005.11.095

Fay, J.A., 2007. Spread of large LNG pools on the sea. *Journal of Hazardous Materials*, 140, 541–551. doi:10.1016/j.jhazmat.2006.10.024

Hansen, O.R., Ichard, M., Davis, S.G., 2009. Validation of FLACS for vapor dispersion from LNG Spills: model evaluation protocol. 12th Annual Symposium, Mary Kay O'Connor Process Safety Center, 712–743.

Horvat A., 2018. CFD methodology for simulation of LNG spills and rapid phase transition (RPT). *Process Safety and Environmental Protection*, 120, 358–369. https://doi.org/10.1016/j.psep.2018.09.025

IMO (International Maritime Organisation), 1997. Resolution MEPC.75(40) Amendments to the Annex of the Protocol of 1978 relating to the International convention for the prevention of pollution from ships, 1973. London: IMO. www.imo.org .

ISO (International Organisation for Standardisation), 2015. ISO/TS 18683: Guidelines for systems and installations for supply of LNG as fuel to ships. Geneva: ISO. https://www.iso.org/standard/63190.html

Jeong, B., Lee, B.S., Zhou, P., Ha, S.-M., 2017. Evaluation of safety exclusion zone for LNG bunkering station on LNG-fuelled ships. *J. Mar. Eng. Technol.* 16 (3), 121–144. https://doi.org/10.1080/20464177.2017.1295786 .

Jeong, B., Lee, B.S., Zhou, P., Ha, S.-M., 2018. Determination of safety exclusion zone for LNG bunkering at fuel-supplying point. *Ocean Eng*. 152, 113–129. https://doi.org/10.1016/j.oceaneng.2018.01.066

Klimenko V. V., 1981. Film boiling on a horizontal plate - new correlation. *Int. J. Heat Mass Transf.*, 24, 69-79. https://doi.org/10.1016/0017-9310(81)90094-6

Luketa-Hanlin A., 2006. A review of large-scale LNG spills: Experiments and modeling. *Journal of Hazardous Materials*. 132, 119-140. DOI: 10.1016/j.jhazmat.2005.10.008

McGrattan, K., et al., 2018. *Fire Dynamics Simulator Technical Reference Guide*. Natl. Inst. Stand. Technol. Spec. Publ. 1018-1.

McGrattan, K., et al., 2020. *PyroSim User Manual v. 2020-2*. Thunderhead Engineering.

Morse, T. L., Kytömaa, H. K., 2011. The effect of turbulence on the rate of evaporation of LNG on water. *J. Loss Prev. Process Ind.*, 24, 791–797. https://doi.org/10.1016/j.jlp.2011.06.004

Park, S., Jeong, B., Young Yoon, J., Paik, J.K., 2018. A study on factors affecting the safety zone in ship-to-ship LNG bunkering. *Ships and Offshore Structures*, 13:sup1, 312-321, DOI: 10.1080/17445302.2018.1461055

Pio G., Carboni M., Iannaccone T., Cozzani V., Salzano E., 2019. Numerical simulation of small-scale pool fires of LNG. *Journal of Loss Prevention in the Process Industries*, 61, 82-88.

Pio G., Salzano E., 2018. Laminar Burning Velocity of Methane, Hydrogen, and Their Mixtures at Extremely Low Temperature Conditions, *Energy & Fuels,* 32, 8830–8836.

Pio G., Salzano, E., 2018. Flammability parameters of liquefied natural gas. *Journal of Loss Prevention in the Process Industries*, 56, 424–429. https://doi.org/10.1016/j.jlp.2018.10.002

Rambøll, 2013. *Risk analysis LNG bunkering of vessels with passengers on board*. Client: DSB, report type joint report, 21/08/2013. https://www.sdir.no/en/shipping/accidents-and-safety/safety-investigations-and-reports/risk-analysis-of-lng-bunkering/

Sagaut P., 2002. Large Eddy *Simulation for Incompressible Flows, second edition*. Springer-Verlag Berlin Heidelberg. ISBN 978-3-662-04697-5.

Sandia, 2014. Guidance on Risk Analysis and Safety Implications of a Large Liquefied Natural Gas (LNG) Spill Over Water. Report SAND2004-6258. https://www.nrc.gov/docs/ML0933/ML093350855.pdf

Scandpower, 2012. *Comparative study on gas dispersion*. Report no. 101368/R1, Date 24 January 2012, Client DSB. https://www.dsb.no/globalassets/dokumenter/rapporter/andre-rapporter/final-report-scandpower-2012.pdf

Sun, B., Guob, K., Pareek, V.K., 2017. Hazardous consequence dynamic simulation of LNG spill on water for ship-to-ship bunkering. *Process Safety and Environmental Protection*, 107, 402-413, http://dx.doi.org/10.1016/j.psep.2017.02.024

Tufano, V., Maremonti, M., Salzano, E., Russo, G. 1998. Simulation of VCEs by CFD modelling: an analysis of sensitivity, *Journal of Loss Prevention in the Process Industries*, 11, 169-175.

Vesovic, V., 2007. The influence of ice formation on vaporization of LNG on water surfaces. *J. Hazard. Mater.*, 140, 518–526. DOI: 10.1016/S0009-2509(00)00110-X

Zhang, Q., Liang, D., 2016. Numerical simulations of LNG vapor dispersion from LNG jetting in different directions. *Procedia Engineering*., 135, 316 – 321. https://doi.org/10.1016/j.proeng.2016.01.136

Zheng J., Chen, L., Wang J., Zhou Y., Wang J., 2019. Thermodynamic modelling and optimization of self-evaporation vapor cooled shield for liquid hydrogen storage tank. *Energy Conversion and Management*., 184, 74-82.

Figure captions

Figure 1. View of 3D geometry for the general layout of the port of Koper 1st basin and old town. Large container ship (in red colour) is shown at berth 7 micro-location with bunker ship (brown colour) on the right. Port area boundaries are shown with purple line. Equidistant red circles are drawn every 25 m from the potential LNG release location.

Figure 2. Wind rose diagram of the case study location (applicable to berth 1 and berth 7 micro-locations).

Figure 3. Evaporative flux profile of LNG from the pool sea surface considered in the FDS and Fluent models (considers conventional evaporation rate 0.18 kg s^{-1} m^{-2}).

Figure 4. UDM modelling obtained UFL, LFL and LFL/2 iso-concentration shapes (in red, green and blue colours, respectively) presented over the orto-photo map of the case area considering four situations. Magenta presents the LNG pool area. Thick circles represent the potential effect zones. Situations A and B apply to the container ship at berth 7, while C and D apply to passenger ship at berth 1 micro-locations; situations A and C consider wind from west-north-west (300°), while situations B and D consider wind from the east-south-east (110°). Note that the bunkering ship is not shown.

Figure 5. UDM, FDS and Fluent modelling obtained LFL and LFL/2 iso-concentration downwind distance vs time profiles for the flat terrain validation case. Note that the case considers the conventional evaporation rate.

Figure 6. UDM, FDS and Fluent modelling obtained LFL and LFL/2 iso-concentration cloud footprint area vs time profiles for the flat terrain validation case. Note that the case considers the conventional evaporation rate.

Figure 7. UDM, FDS and Fluent modelling obtained LFL and LFL/2 iso-concentration cloud height vs distance downwind profiles, at 160 s from the start of the release, for the flat terrain validation case. Note that the case considers the conventional evaporation rate.

Figure 8. FDS modelling obtained views to the methane concentrations for the first micro-simulation (container terminal, wind from west-north-west (300°), conventional evaporation rate). Please note arrow with "wind" representing wind direction in the first image.

Figure 9. FDS and Fluent modelling obtained LFL iso-concentration cloud downwind distances and cloud area vs time profiles for first micro-simulation (container terminal, wind from west-north-west (300°), conventional evaporation rate).

Figure 10. FDS modelling obtained views to the methane concentrations for the second micro-simulation (passenger terminal, wind from the east-south-east (110°), conventional evaporation rate).

Figure 11. FDS and Fluent modelling obtained LFL iso-concentration cloud downwind distances and cloud area vs time profiles for second micro-simulation (passenger terminal, wind from the east-south-east (110°), conventional evaporation rate).

Figure 12. FDS modelling obtained views to the methane concentrations third micro-simulation (passenger terminal, wind from west-north-west (300°), conventional evaporation rate).

Figure 13. FDS and Fluent modelling obtained LFL iso-concentration cloud downwind distances and cloud area vs time profiles for third micro-simulation (passenger terminal, wind from west-north-west (300°), conventional evaporation rate).

Figure 14. Alternative evaporation flux profile of LNG from the pool sea surface considered in the FDS and Fluent models (considers alternative evaporation rate 0.053 kg s^{-1} m^{-2}).

Figure 15. FDS modelling obtained views to the methane concentrations for fourth micro-simulation (container terminal, wind from west-north-west (300°), alternative evaporation rate).

Figure 16. FDS and Fluent modelling obtained LFL iso-concentration cloud downwind distances and cloud area vs time profiles for fourth micro-simulation (container terminal, wind from west-north-west (300 °), alternative evaporation rate).

Figure 17. FDS modelling obtained LFL iso-concentration cloud downwind distances and cloud area vs time profiles for conventional and alternative LNG evaporation rates - comparison of scenarios 1 and 4 (container terminal, wind from west-north-west (300°).

Figure 18. Fluent modelling obtained LFL iso-concentration cloud downwind distances and cloud area vs time profiles for conventional and alternative LNG evaporation rates – comparison of scenarios 1 and 4 (container terminal, wind from west-north-west (300°).

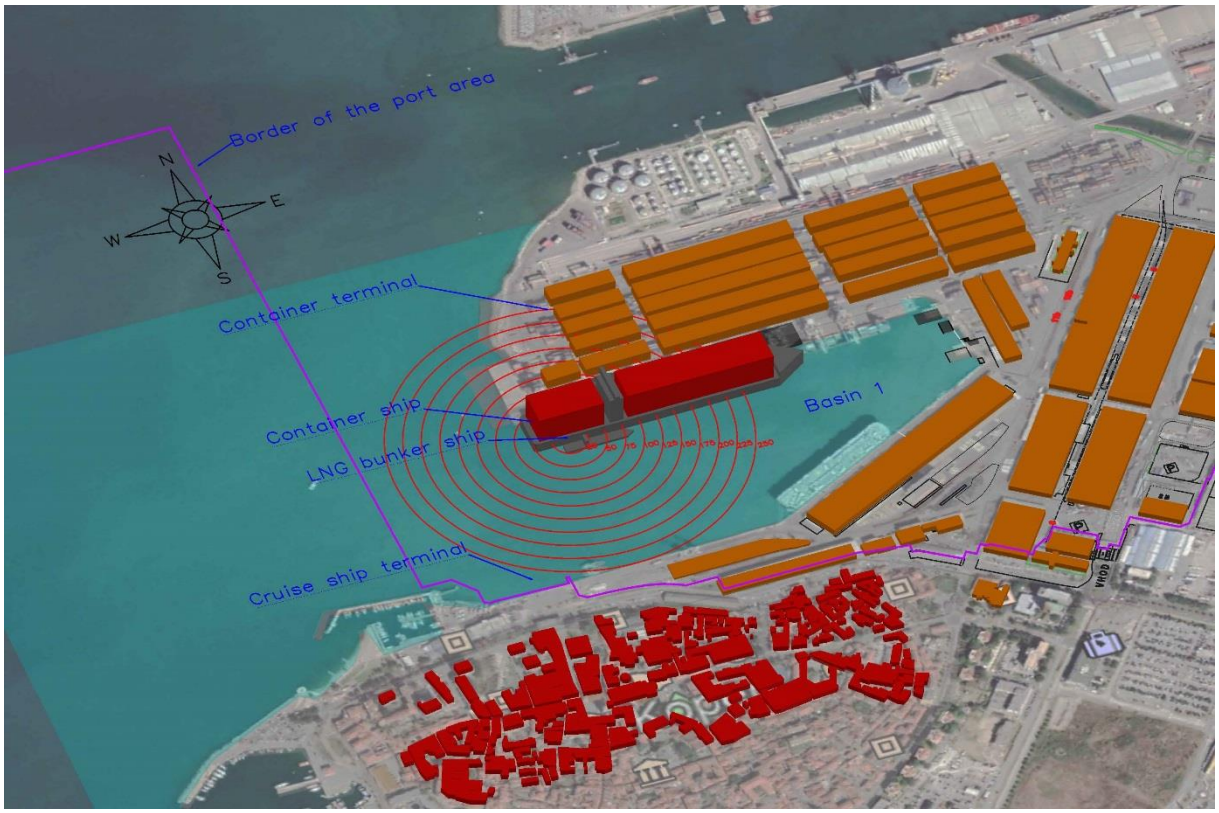

Figure 1

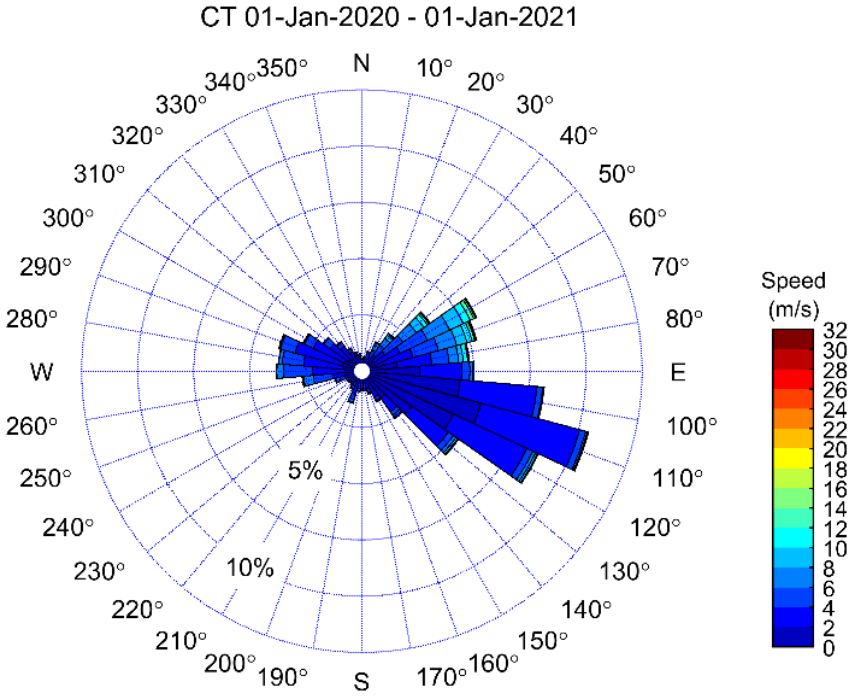

Figure 2

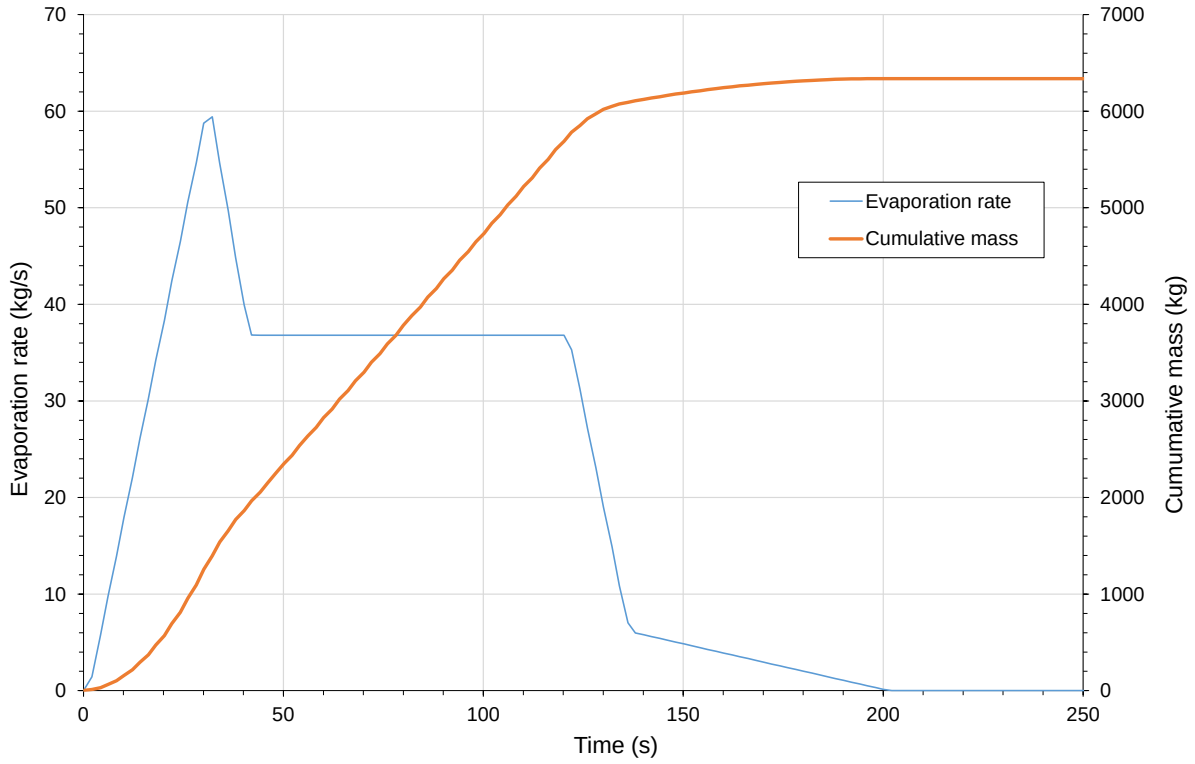
Evaporation rate (kg/s)
Cumumative mass (kg)
Time (s)
Evaporation rate
Cumulative mass
0
10
20
30
40
50
60
70
0
1000
2000
3000
4000
5000
6000
7000
0
50
100
150
200
250

Figure 3

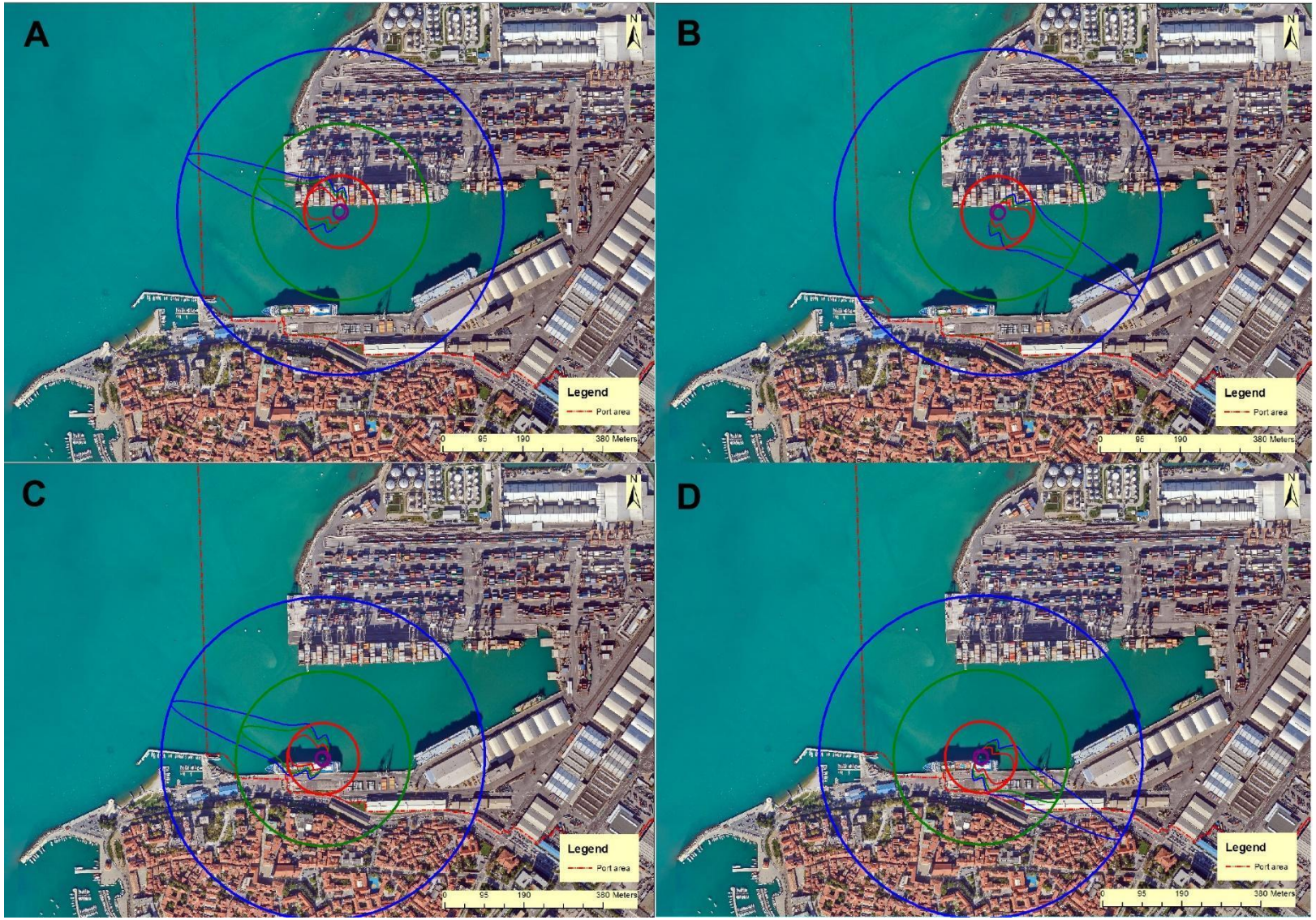

Figure 4

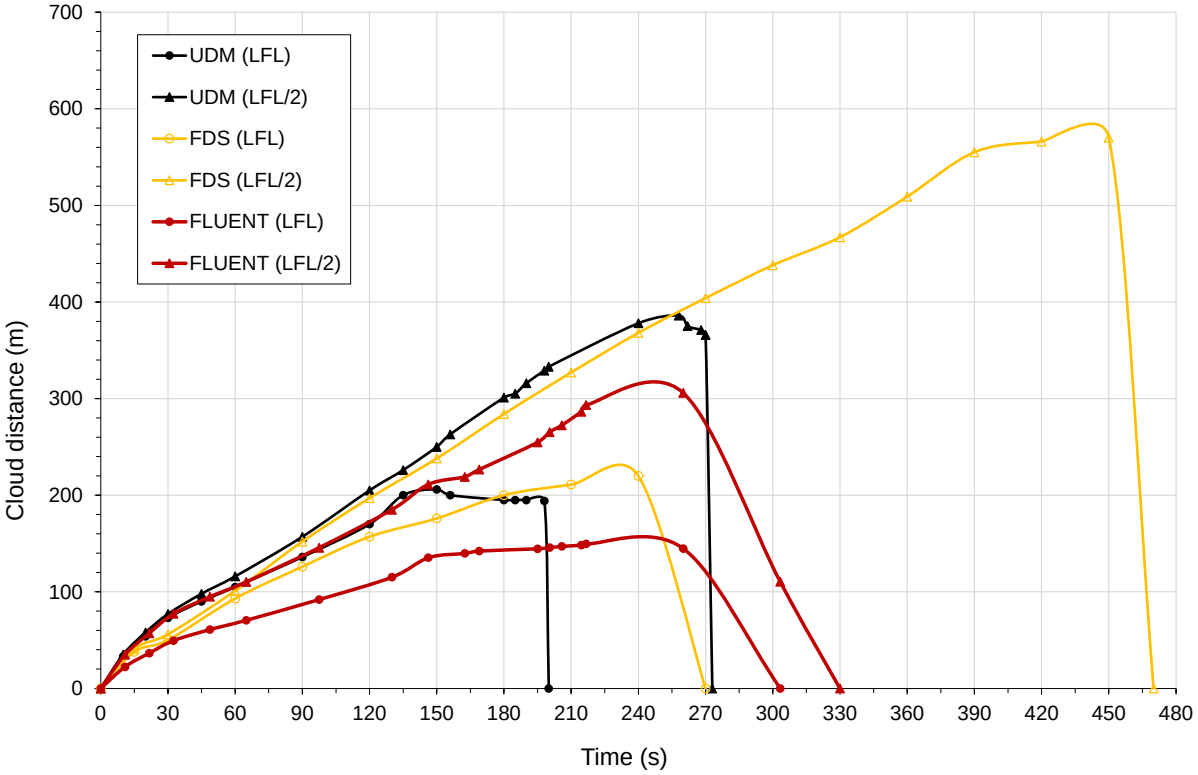

Figure 5

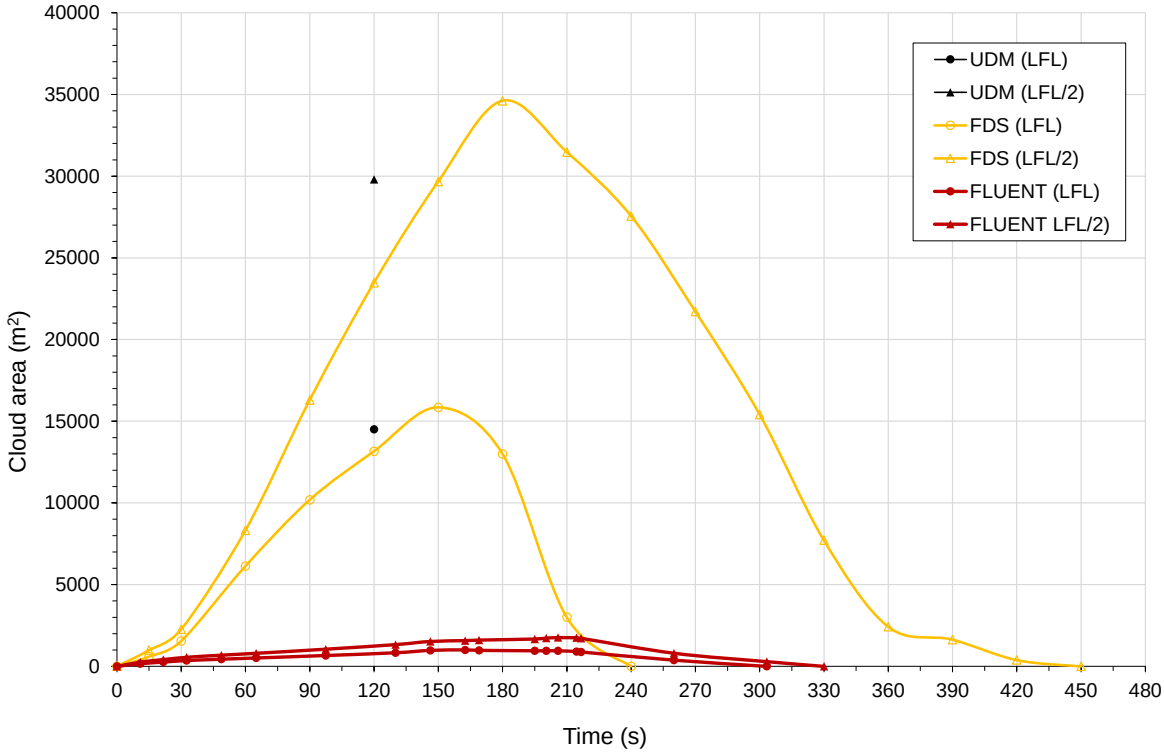

Figure 6

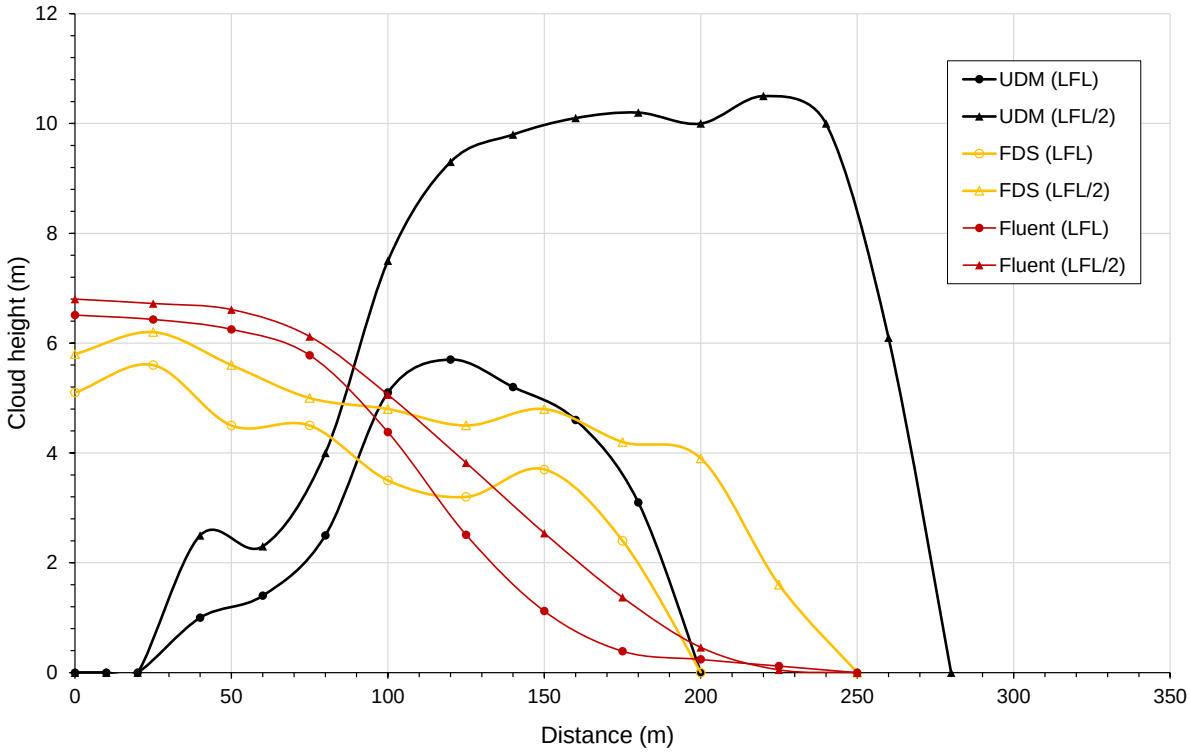
Cloud height (m)
Distance (m)
0
2
4
6
8
10
12
0
50
100
150
200
250
300
350
UDM (LFL)
UDM (LFL/2)
FDS (LFL)
FDS (LFL/2)
Fluent (LFL)
Fluent (LFL/2)

Figure 7

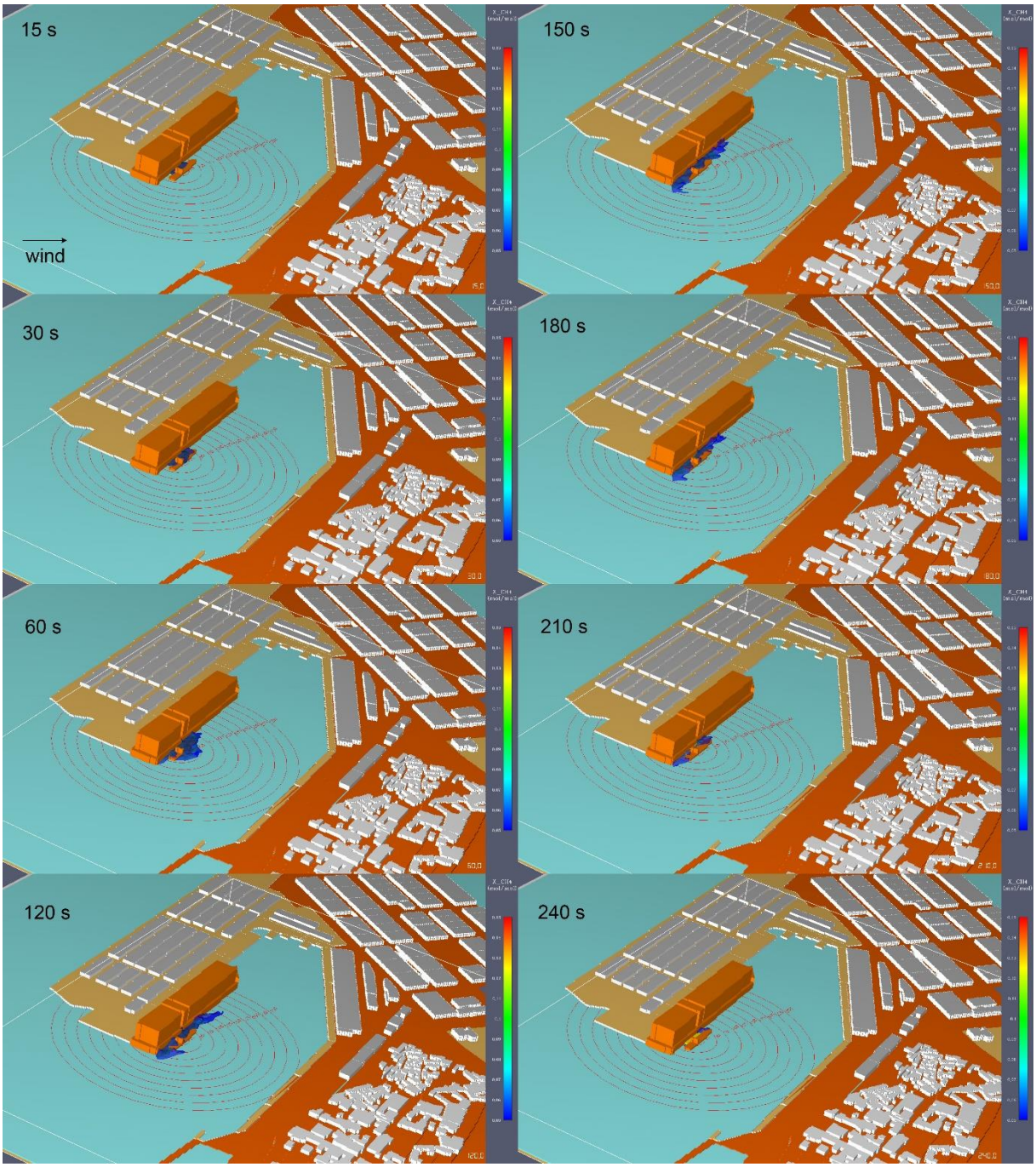

Figure 8

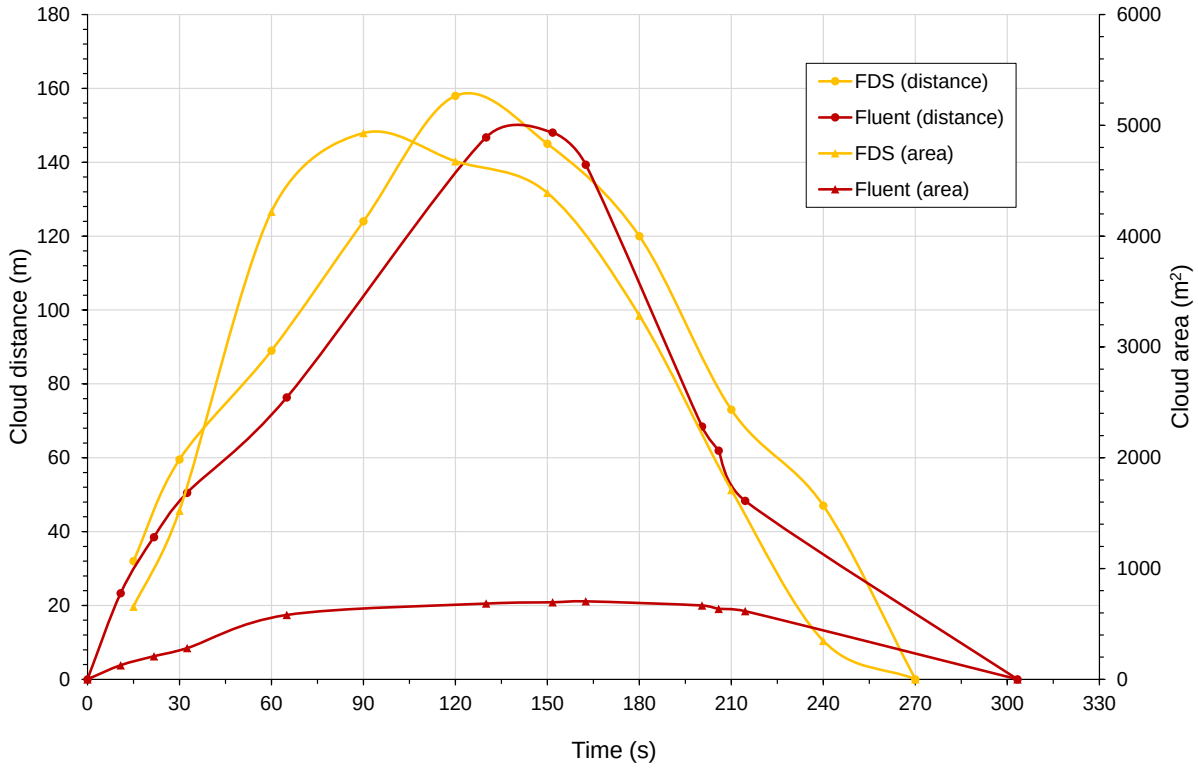
FDS (distance)
Fluent (distance)
FDS (area)
Fluent (area)
Cloud distance (m)
Cloud area (m²)
Time (s)
0
20
40
60
80
100
120
140
160
180
0
1000
2000
3000
4000
5000
6000
0
30
60
90
120
150
180
210
240
270
300
330

Figure 9

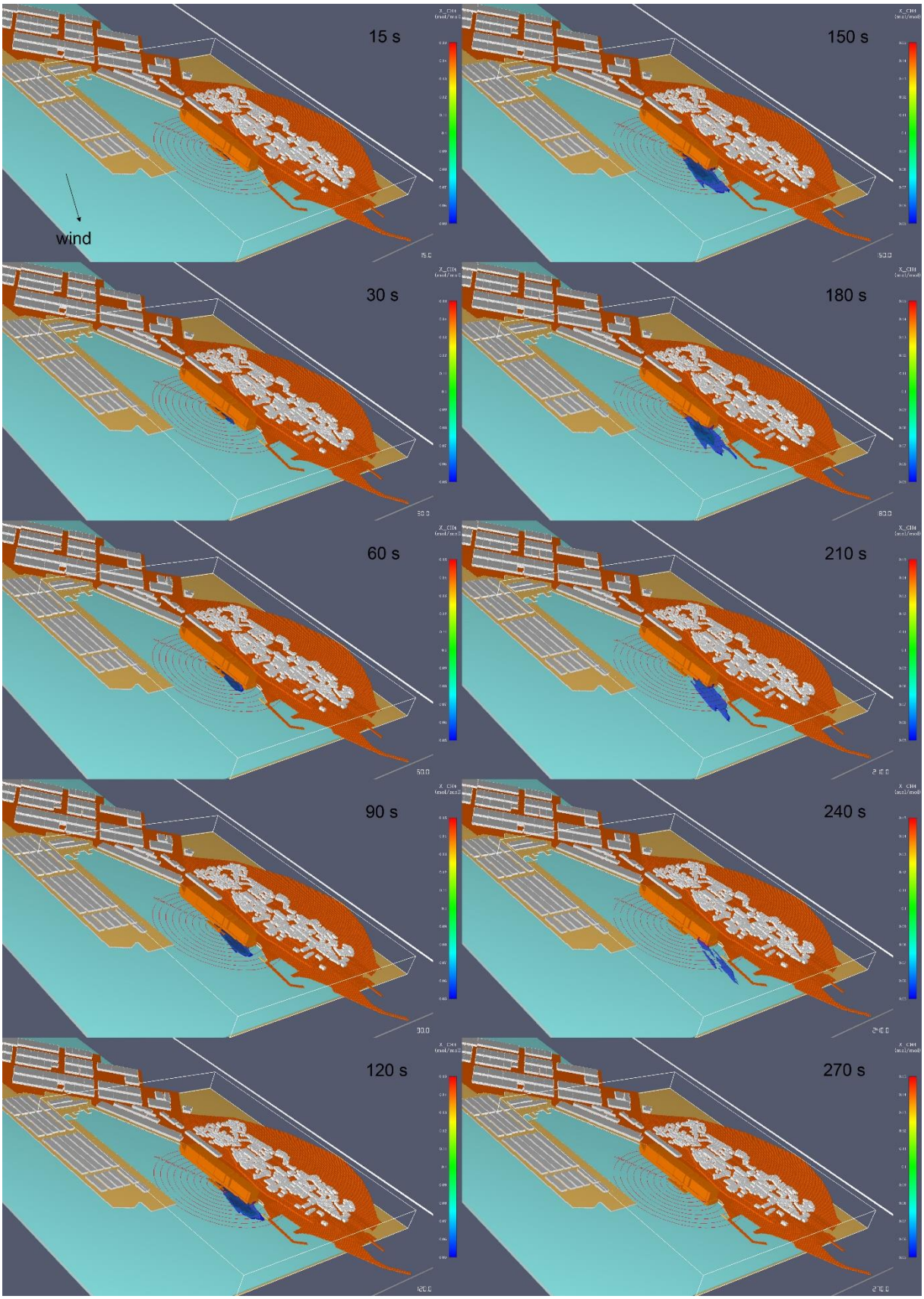

Figure 10

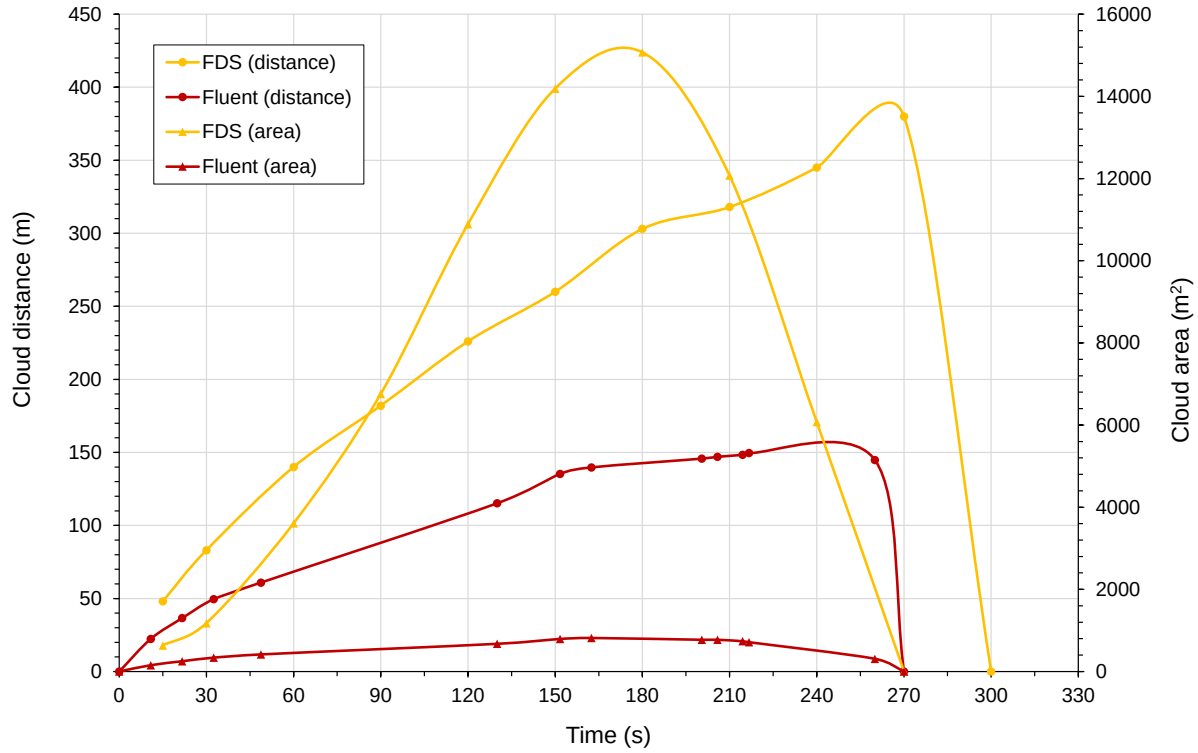
FDS (distance)
Fluent (distance)
FDS (area)
Fluent (area)
Cloud distance (m)
Cloud area (m²)
Time (s)
0
50
100
150
200
250
300
350
400
450
0
2000
4000
6000
8000
10000
12000
14000
16000
0
30
60
90
120
150
180
210
240
270
300
330

Figure 11

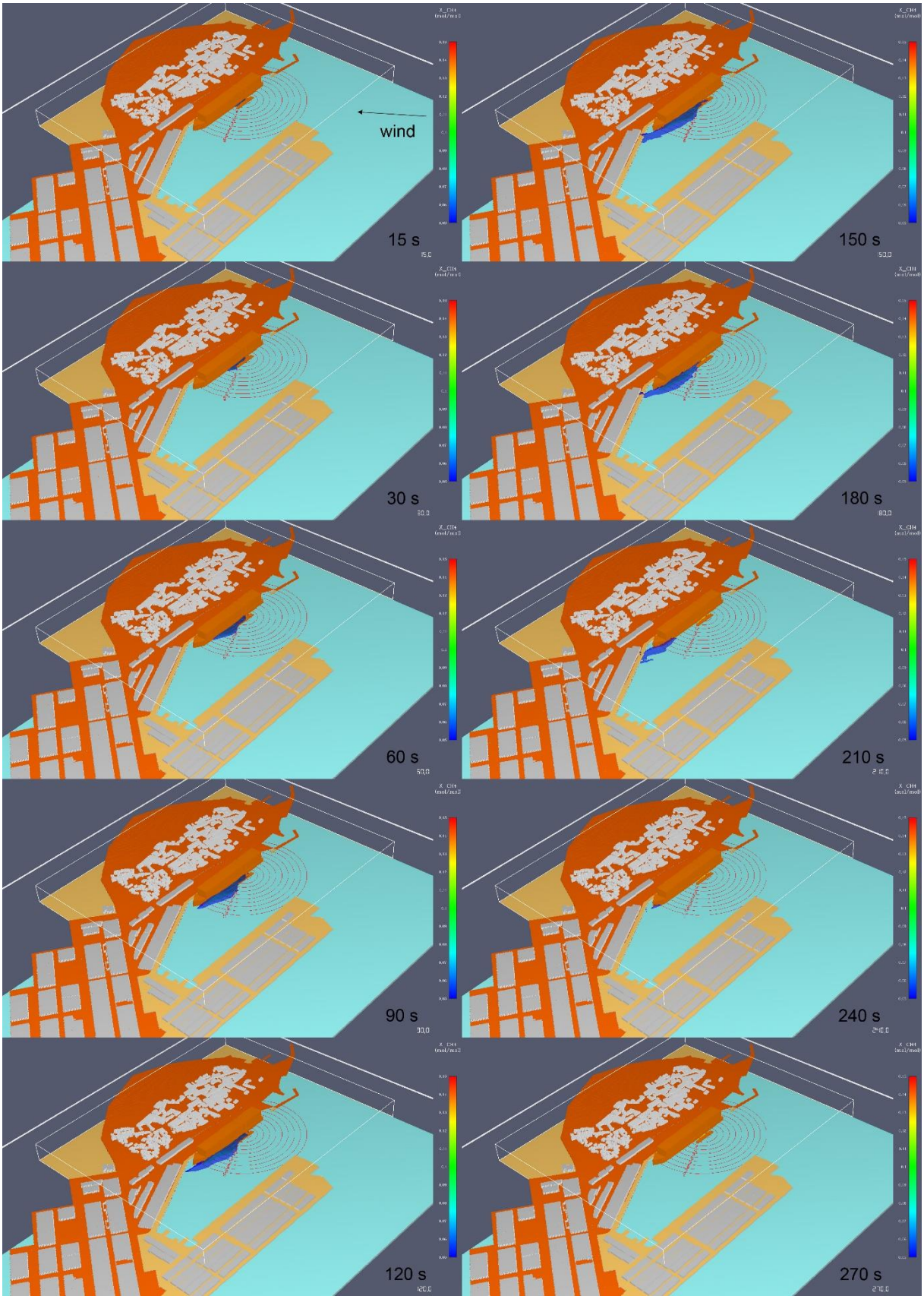

Figure 12

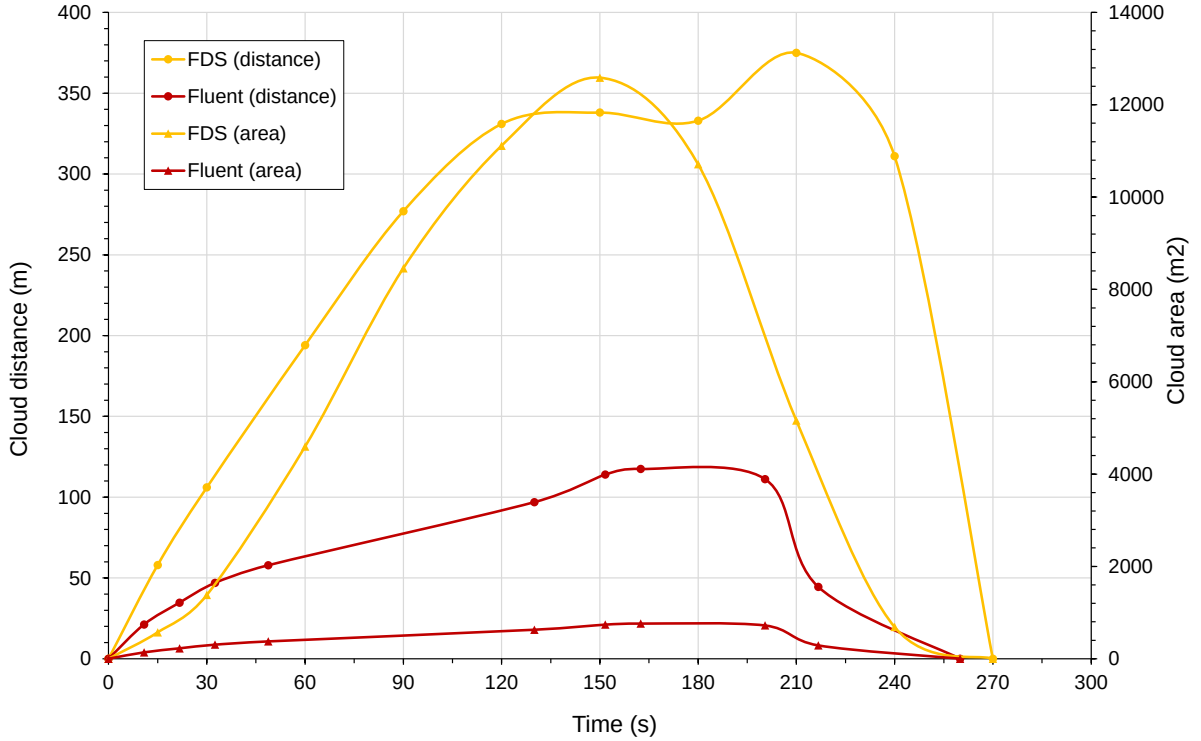

Figure 13

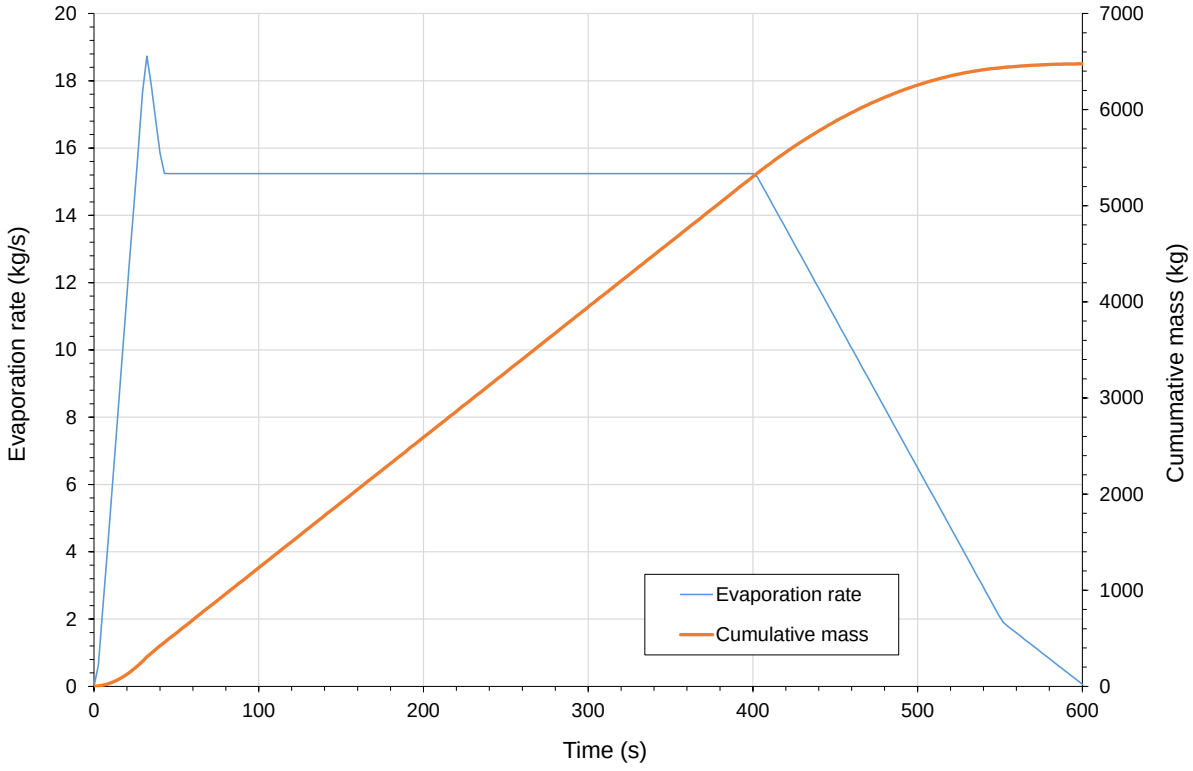

Figure 14

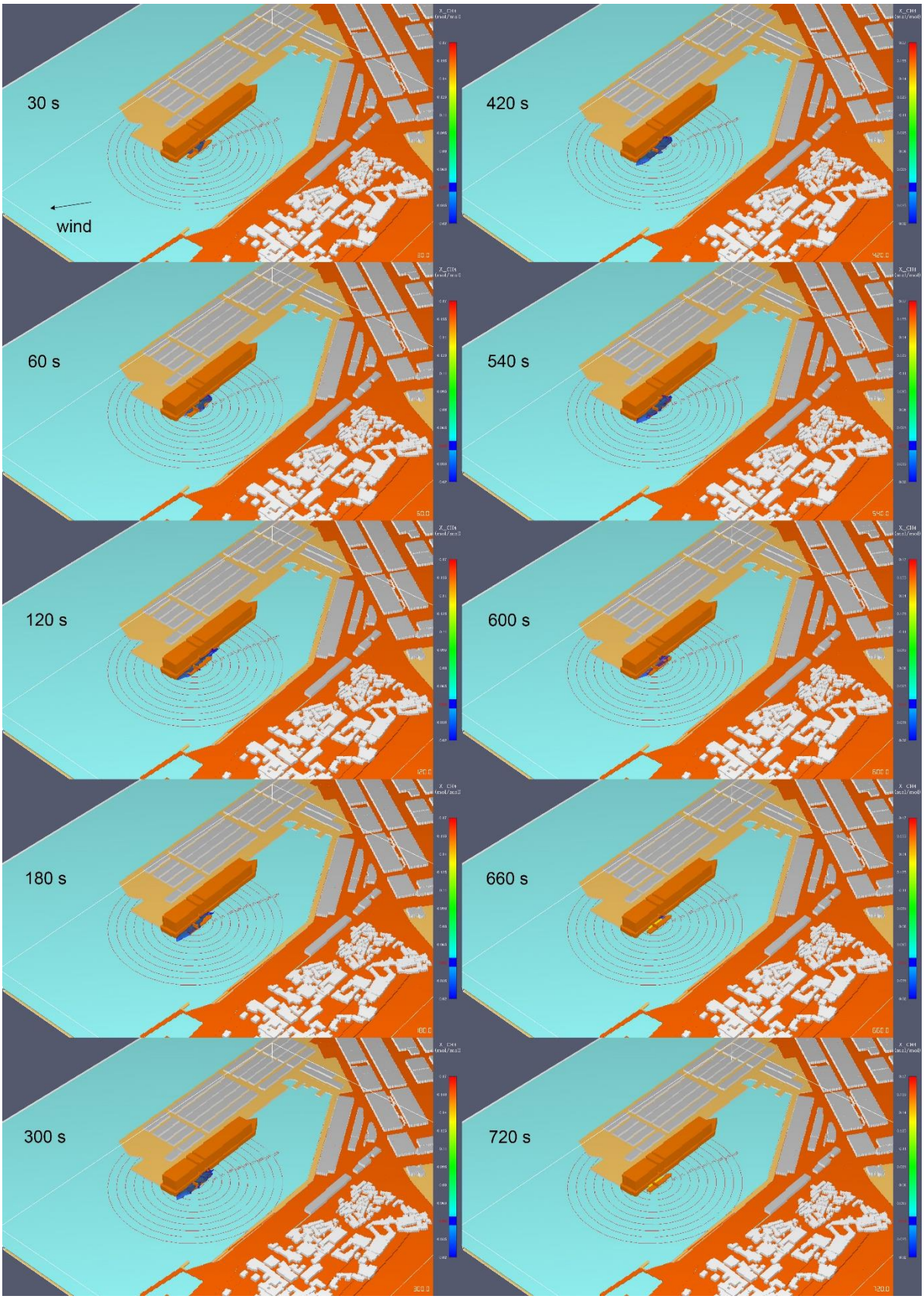

Figure 15

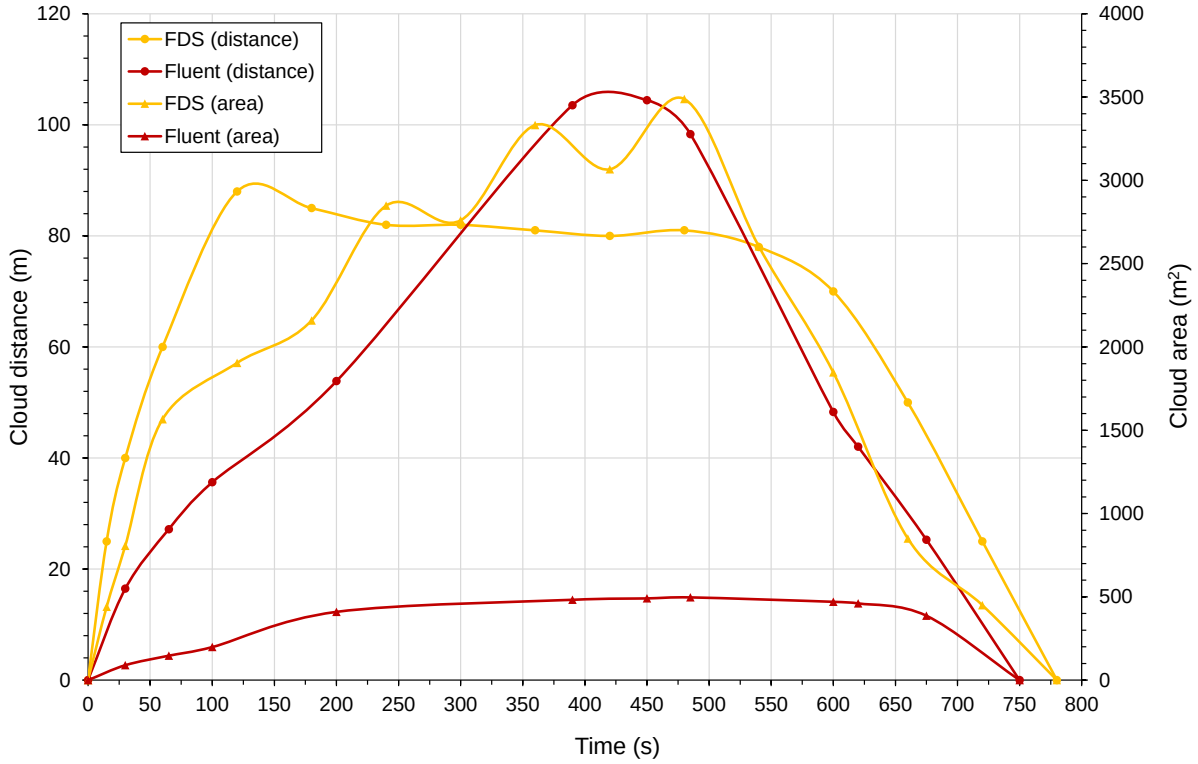
FDS (distance)
Fluent (distance)
FDS (area)
Fluent (area)
Cloud distance (m)
Cloud area (m²)
Time (s)
0
20
40
60
80
100
120
0
500
1000
1500
2000
2500
3000
3500
4000
0
50
100
150
200
250
300
350
400
450
500
550
600
650
700
750
800

Figure 16

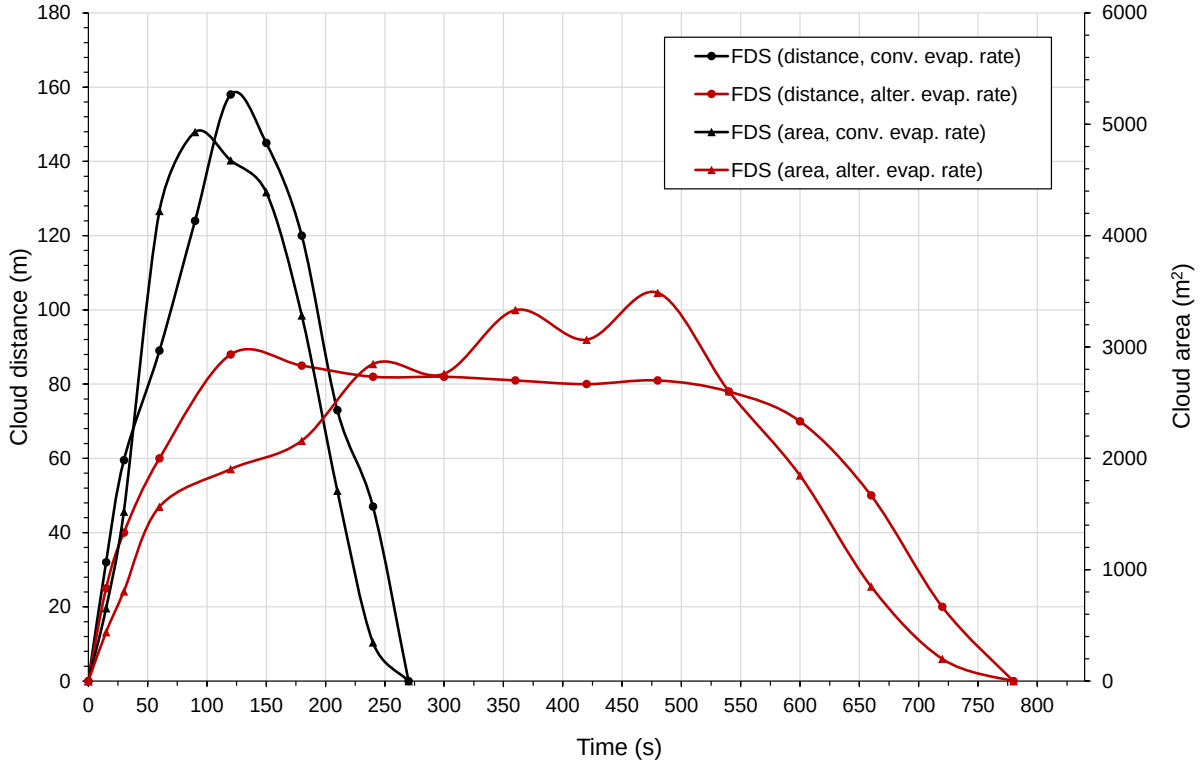

Figure 17

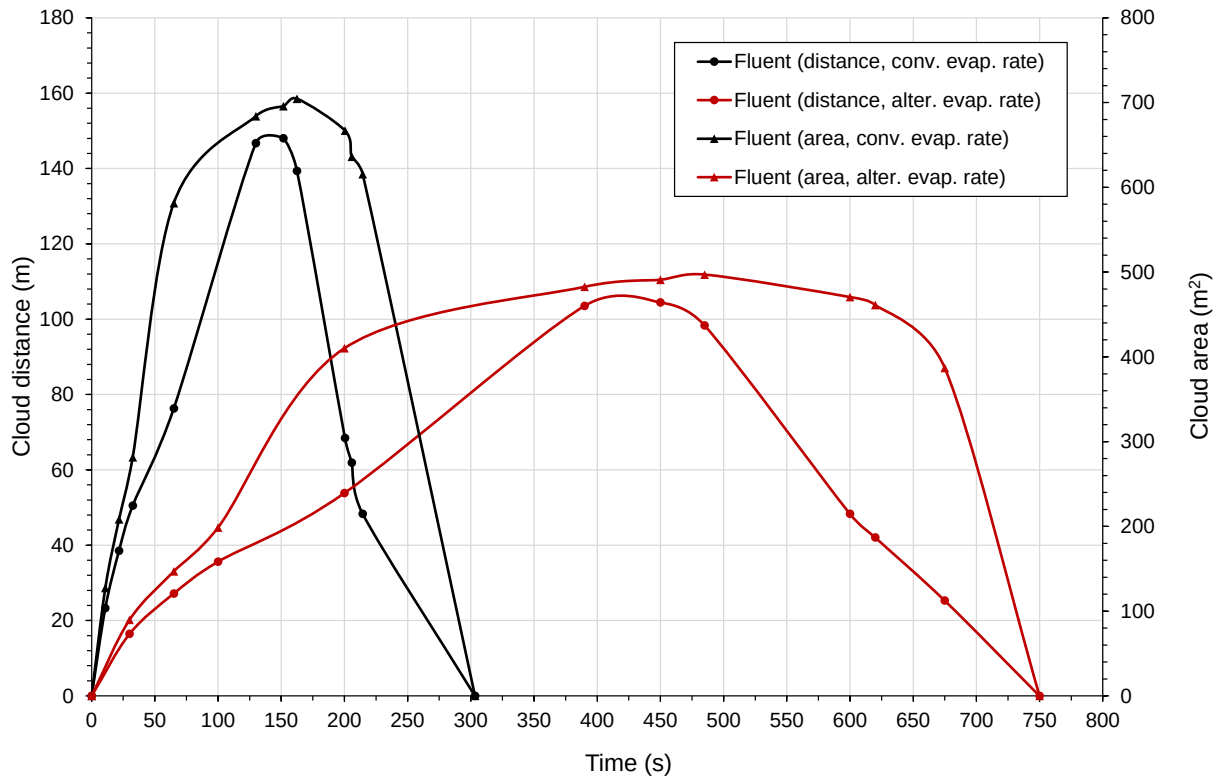

Figure 18

Table 1. Summary of important modelling parameters of the release scenario.

Parameter	Unit	Value
Source term data		
Model substance released	-	methane
Temperature	°C	-164
Pressure difference at the release point (head)	bar	6
Hose diameter	mm	150
Release rate	kg s^{-1}	53.2
Release duration	s	120
Meteorological situation		
Wind speed	m s^{-1}	2
Wind stability category (PG)	-	D
Wind direction(s)	°	east-south-east (110°); west-north-west (300°)
Air temperature	°C	25
Location data		
Substrate type	-	deep water [a]
Bund presence	-	none
Substrate temperature	°C	20
Substrate surface roughness parameter (z_0)	m	0.005

Notes: [a] – a channel with open both ends is formed between both ships (UDM model).

Table 2. Summary of UDM modelling results for the release scenario

Parameter	Unit	Value
Max. downwind distance to the concentration of interest [a]		
UFL	m	85
LFL	m	231
LFL/2 [b]	m	420
LNG pool formed on the sea		
Max. diameter (considering early/late ignition)	m	14/28
Max./stationary pool inventory	kg	540/120
Time till pool reaches a stationary diameter	s	40
Overall pool duration	s	135

Note:

[a] – Results are the same for both wind directions (from east-south-east and west-north-west).

[b] – Flammable cloud duration is about 290 s.